High-resolution numerical simulations of resuspending gravity currents: conditions for self-sustainment

F. Blanchette,[1] M. Strauss,[2] E. Meiburg,[1] B. Kneller,[3] M.E. Glinsky[4]

F. Blanchette Department of Mechanical and Environmental Engineering, University of California, Engineering II, room 2355, Santa Barbara, CA 93106, USA. (blanchef@engr.ucsb.edu)

[1]Department of Mechanical and Environmental Engineering, University of California, Santa Barbara, California, USA.

[2]Nuclear Research Center, Negev, Beer Sheva, Israel.

[3]Institute for Crustal Studies, University of California, Santa Barbara, California, USA.

[4]BHP Billiton Petroleum, Houston, Texas, USA

Abstract. We present highly resolved two-dimensional simulations of particle-laden gravity currents and focus on the influence of particle entrainment from the underlying bed. We model particle resuspension as a diffusive flux of particles through the bottom boundary. As turbulent motions detach particles from the bottom surface, resuspension induced over the body of the current is transfered to the current's head, causing it to become denser and potentially accelerating the front of the current. The conditions under which turbidity currents may become self-sustaining through particle entrainment are investigated as a function of slope angle, current and particle size, and particle concentration. The effect of computational domain size and initial aspect ratio of the current on the evolution of the current are also considered. Applications to flows traveling over a surface of varying slope angle, such as turbidity currents spreading down the continental slope, are modeled via a spatially varying gravity vector. Particular attention is given to the resulting particle deposits and erosion patterns.

1. Introduction

Gravity currents are flows generated when a predominantly horizontal density gradient is present in a fluid and hydrostatic pressure differences cause the heavy fluid to spread underneath the light fluid. In geophysical contexts, the density difference between the current and the ambient fluid is often due to the presence of suspended particles which act as the current's driving force. Such particles also settle relative to the fluid and may deposit at the bottom edge of the current. In particular, the dynamics of particle-laden gravity currents are relevant to ash-laden volcanic flows (Sparks *et al.* 1991), crystal laden flows in magma chambers (Hodson 1998) and turbidity currents, i.e. underwater currents in which the excess density is provided by suspended sediment (Simpson 1997).

Erosion by turbidity currents is largely responsible for the creation of submarine canyons on continental slopes (e.g. Pratson & Coakley 1996). Turbidity currents are the most significant agents of sediment transport into the deep sea, creating accumulations that include the Earth's largest sediment bodies (Normark *et al.* 1993). They also constitute a hazard to marine engineering installations such as oil platforms, pipelines and submarine cables (Krause *et al.* 1970). Natural turbidity currents occur infrequently and unpredictably in remote and hostile environments, and tend to be destructive of submarine monitoring equipment (e.g. Zeng *et al.* 1991). Consequently they are observed only rarely and generally by indirect means only (Hay *et al.* 1982; Hughes-Clarke *et al.* 1990). Laboratory and numerical experiments thus constitute essential means of investigating these important large scale natural phenomena.

Particle-laden gravity currents have been studied intensively in the past four decades. Turbidity currents are non-conservative in that they entrain ambient fluid through turbulent mixing, and deposit sediment as turbulent motions decay. They may also erode sediment from the bed, thus producing self-sustaining ("auto-suspending" or "ignitive") currents (Parker *et al.* 1986; Pantin 1991, 2001). Simplified analytical models have been suggested to describe density currents (Huppert & Simpson 1980) and the asymptotic limit of small particle concentration was considered by using density-driven gravity currents as a known background flow (Hogg *et al.* 2000). Experimental studies of the progression of particle-laden currents with finite volume (Bonnecaze *et al.* 1993) or constant flux (García & Parker 1993) were performed, and particular attention was given to the resulting deposits. Layer-averaged numerical models have been suggested by Bonnecaze *et al.* (1993) and García & Parker (1993). Such simplified models require a number of closure assumptions regarding bottom friction, bottom shear stress, fluid entrainment and front velocity. More recently, highly resolved two- and three-dimensional simulations computing fluid flow from first principles have successfully described particle-laden gravity currents (Necker *et al.* 2002). Several features of the flow, such as energy and particle concentration distribution may easily be computed from these simulations and significantly fewer closure assumptions are required in such models. For those reasons, a similar approach is used in the present study to model resuspending gravity currents.

The geometry of the surface over which currents propagate determines their long term behavior. For density currents, experimental studies of the influence of the slope angle were performed by Britter & Linden (1980) and Beghin *et al.* (1981).

Particle-laden currents traveling down a broken slope were investigated by García (1993) owing to their relevance to turbidity currents spreading down the continental shelf before reaching a relatively flat ocean bottom. Complex geometries were recently included in highly resolved simulations via the inclusion of a spatially varying gravity vector in a rectangular computational domain (Blanchette *et al.* 2004). If a current is spreading over an erodible bed, the geometry of the base may allow the current to resuspend sufficient particles so that its mass and velocity increase as it progresses down slope. This phenomenon is responsible for the destructive power of avalanches (Hutter 1996). Self-sustaining turbidity currents are known to occur in the oceans where they may travel over hundreds of kilometers, as exemplified by the Grand Banks turbidity current of 1929 (Heezen & Ewing 1952).

The flux of resuspended particles as a function of flow and particle parameters is particularly difficult to estimate. Several empirical models have been suggested (Smith & McLean 1977, García & Parker 1991, 1993) but their applicability remains limited and they must be used with caution. At present, it is fair to say that particle resuspension is not fully understood. However, since reentrainment of particles is critical in the long term behavior of gravity currents, it must be taken into account despite the limitations inherent in empirical models.

Our study focuses on the conditions required for a particle-laden current to exhibit a snow ball effect and on the depositional and erosional properties of such currents. We use highly resolved, two-dimensional simulations of particle-laden gravity currents (Necker *et al.* 2003) combined with an empirical resuspension model (García & Parker 1993) to characterize the evolution gravity currents propagating over an erodible bed.

We determine under which conditions a current becomes self-sustaining depending on parameters such as the particle size and concentration, current height and slope angle. Our model and numerical approach are presented in §2. We describe our results in §3, and the implications of our findings are discussed in §4.

2. Model Description

2.1. Governing Equations and Relevant Parameters

We consider currents in which the particle concentration is relatively low, so that particle-particle interactions may be neglected. The density difference between the current and the ambient is thus typically small and we may use the Boussinesq approximation (e.g. Spiegel & Veronis 1960), where density variations appear only in the buoyancy term. We use a continuum approach, where the density of the suspension, $\bar{\rho}$, is related to the particle concentration by volume, $\bar{C}$, through $\bar{\rho} = \bar{\rho}_f + \bar{C}(\bar{\rho}_p - \bar{\rho}_f)$, where $\bar{\rho}_f$ and $\bar{\rho}_p$ are the fluid and particle density, respectively, and the bars indicate dimensional quantities. Particles are assumed to be transported by the fluid and to settle relative to the fluid with velocity $\bar{U}_s$ in the direction of gravity.

To reduce computation time, we restrict our attention to two-dimensional systems. We eliminate pressure terms by considering a stream function-vorticity description of the fluid motion. Denoting the coordinate parallel to the bottom surface by x_1, that perpendicular by x_2 and the corresponding velocities by u_1 and u_2 respectively (see figure **??**), we introduce a stream function ψ satisfying $u_1 = \partial\psi/\partial x_2$ and $u_2 = -\partial\psi/\partial x_1$ and a vorticity function $\omega = \partial u_2/\partial x_1 - \partial u_1/\partial x_2$.

We use the initial half-height of the suspension reservoir, $\bar{h}$, as a length scale, and the initial particle concentration, $\bar{C}_0$, as a concentration scale. As a typical velocity, we consider the buoyancy velocity

$$\bar{u}_b = (g\bar{h}\bar{C}_0 R)^{1/2}, \tag{1}$$

where g is the gravitational acceleration and $R = (\bar{\rho}_p - \bar{\rho}_f)/\bar{\rho}_f$. We thus obtain the following non-dimensional governing equations (Necker *et al.* 2002)

$$\nabla^2\psi = -\omega \tag{2}$$

$$\frac{D\omega}{Dt} = \frac{\nabla^2\omega}{Re} - \frac{\partial(C\cos\theta)}{\partial x_1} - \frac{\partial(C\sin\theta)}{\partial x_2} \tag{3}$$

$$\frac{DC}{Dt} + U_s\left(\frac{\partial(C\sin\theta)}{\partial x_1} - \frac{\partial(C\cos\theta)}{\partial x_2}\right) = \frac{\nabla^2 C}{Pe}, \tag{4}$$

where we use the notation $D/Dt = \partial/\partial t + u_1\partial/\partial x_1 + u_2\partial/\partial x_2$ and where $U_s = \bar{U}_s/\bar{u}_b$, $Re = \bar{u}_b\bar{h}/\bar{\nu}$ is the Reynolds number and $Pe = \bar{u}_b\bar{h}/\bar{\kappa}$ the Péclet number, with $\bar{\nu}$ the fluid viscosity and $\bar{\kappa}$ the particle diffusion constant.

Our simulations aim at reproducing as closely as possible the physical conditions prevailing in large turbidity currents. We therefore elected to simulate currents in which water is the suspending fluid, i.e. $\bar{\rho}_f = 1\text{g/cm}^3$ and $\bar{\nu} = 10^{-6}\text{m}^2/\text{s}$. We consider particles of density $\bar{\rho}_p = 2.5\text{g/cm}^3$ ($R = 1.5$) and typical diameter $\bar{d} = 100\mu\text{m}$, values appropriate for sandy turbidity currents such as those forming many submarine fans (Normark *et al.* 1993). To compute the particle settling speed we employ the empirical formula of Dietrich (1982), $\bar{U}_s = (W g R \bar{\nu})^{1/3}$, where

$$\begin{aligned} W &= 1.71 \times 10^{-4}\left(\frac{gR\bar{d}^3}{\bar{\nu}^2}\right)^2, && \text{if } \lambda < -1.3 \\ &= 10^{p(\lambda)}, && \text{otherwise,} \end{aligned}$$

with $\lambda = \log_{10}(gR\bar{d}^3/\bar{\nu}^2)$ and $p(\lambda) = (-3.76715 + 1.92944\lambda - 0.09815\lambda^2 - 0.0057\lambda^3 + 0.00056\lambda^4)$. To compute the buoyancy velocity, we use a typical particle concentration of $\bar{C}_0 = 0.5\%$ and height of approximately $\bar{h} = 1.6$m, which results in a non-dimensional particle settling speed of $U_s = 0.02$.

The parameters previously mentioned correspond to a current Reynolds number of order 10^6, which is well beyond the current reach of numerical simulations. As Re increases, smaller length scales must be resolved, which in turn implies shorter time steps. We are therefore constrained to use reduced values of the Reynolds number to allow for reasonable computation times. We consider a turbulent Reynolds number, $Re_T = \bar{u}_b\bar{h}/\nu_e$, where ν_e is the effective viscosity of the flow due to turbulent motions. We expect $\nu_e \gg \bar{\nu}$ and consequently $Re_T \ll Re$. As a first approximation, we assume Re_T to be constant. More complete turbulence models, such as a $K-\epsilon$ model (Speziale 1991, Choi & García 2002), could allow for a more precise description of the evolution of the turbulence. However, in the presence of suspended particles, the several empirical coefficients needed in the $K-\epsilon$ model are not well established and need to be empirically determined. Such an approach exceeds the scope of the present work and is left for future considerations. Using a turbulent Reynolds number of the order of a few thousands is generally thought to be a valid approximation to large Reynolds number flows (Parsons & García 1998). In this regime, the main features of the flow are almost independent of Re_T, as discussed further in §3.1.

Similarly, numerical considerations limit the size of the Péclet number we may simulate. We here suggest that turbulent motions, on a scale smaller than that which may be resolved in our simulations, act to diffuse the particle concentration. We thus define a turbulent Péclet number, $Pe_T = \bar{u}_b\bar{h}/\kappa_e$, where κ_e is an effective particle diffusivity. Since we expect that turbulent motions diffuse momentum and particle concentration in a similar manner (Shraiman, 2000), the natural choice is to select $\nu_e = \kappa_e$ and therefore $Pe_T = Re_T$.

We use a lock-release model, where heavy fluid is initially confined to a small region, $0 \leq x_1 \leq x_f$ and $0 \leq x_2 \leq 2$. The initial length of the current, x_f, may be varied but was usually kept at $x_f = 2$. For reasons of numerical stability, the initial concentration profile was smoothed over a few grid points (typically 6) using an error function centered at $x_1 = x_f$ in the horizontal and at $x_2 = 2$ in the vertical. The fluid is initially at rest, $\psi = \omega = 0$ and starts moving at $t = 0$.

In order to model complex geometries, we use a spatially varying gravity vector (Blanchette *et al.* 2004). A curvilinear coordinate system is thus simulated but second order curvature terms are neglected. The resulting approximation is expected to be valid if the ratio of the height of the flow to the radius of curvature of the bottom surface is everywhere small. We restrict our study to smoothly varying bottom surfaces to ensure that the neglected curvature effects remain small. We use a rectangular computational domain and enforce a no-slip, no normal flow condition at the top and bottom boundaries, $\psi = \partial\psi/\partial x_2 = 0$, and a slip, no normal flow condition at the left and right walls, $\psi = \partial^2\psi/\partial x_1^2 = 0$. The latter conditions allow for the use of fast Fourier transforms in the x_1-direction which provide high accuracy to our numerical scheme.

The particle concentration flux at the boundaries, F, is set to zero at the top and left walls. At the right wall, which effectively is never reached by the heavy current, particles may deposit, but no resuspension is allowed so that $F = -CU_s \cos\theta$. However, particles are allowed to deposit and reenter suspension at the bottom boundary:

$F = (-CU_s \cos\theta + E_s U_s)$, where E_s is a measure of the resuspension flux as discussed below. Unresolved turbulent motions are assumed to be responsible for resuspending particles near the bottom boundary. The influx of particles due to resuspension is therefore modeled as a turbulent diffusive flux, as small scale turbulent motions bring deposited particles into the suspension. The height of the deposit, $d(x_1, t)$, may be found by integrating the particle flux over time

$$d(x_1, t) = \frac{\bar{C}_0}{\sigma} \int_0^t (CU_s \cos\theta \mid_{x_2=0} - E_s U_s) dt,$$

where σ is the particle volume fraction in the bed, taken to be a constant $\sigma = 0.63$ (Torquato *et al.* 2000). Note that the corresponding porosity of the deposit is $1 - \sigma = 0.37$.

To evaluate the resuspension flux, $E_s U_s$, we use the empirical formula of García & Parker (1993) which relates the resuspension flux to the particle Reynolds number and bottom shear velocity. We consider an erodible bed composed of particles identical to those in suspension. A measure of the vigor of the resuspension is given by Z, which, following García & Parker (1993), is defined as

$$Z = \frac{u^*}{U_s} Re_p^{0.6} \quad \text{if } Re_p > 2.36,$$
$$Z = 0.586 \frac{u^*}{U_s} Re_p^{1.23} \quad \text{if } Re_p \le 2.36$$

where u^* is the shear velocity at the bottom wall and Re_p is the particle Reynolds number

$$u^* = \left(\frac{1}{Re_T} \left. \frac{\partial u}{\partial x_2} \right|_{x_2=0} \right)^{1/2}, \qquad Re_p = \frac{\bar{d}(g\bar{d}R)^{1/2}}{\bar{\nu}}. \tag{5}$$

The lower and upper branches of Z reflect the different settling dynamics of low and high particle Reynolds numbers, respectively. The resuspension flux, $E_s U_s$, is then a threshold function of Z,

$$E_s = \frac{1}{\bar{C}_0} \frac{aZ^5}{1 + \frac{a}{0.3} Z^5}, \tag{6}$$

with $a = 1.3 \times 10^{-7}$. Notice that the normalization of E_s by the initial particle concentration renders the effect of resuspension more significant for dilute suspensions. Also, E_s may not exceed $0.3/\bar{C}_0$, thus providing a saturation mechanism.

Thus, at the top and left boundaries the diffusive flux is equal to the settling flux, it is zero at the right wall and it is equal to the resuspension flux at the bottom surface:

$$CU_s \cos\theta + \frac{1}{Pe_T} \frac{\partial C}{\partial x_2} = 0 \quad \text{at } x_2 = H, \tag{7}$$

$$-CU_s \sin\theta + \frac{1}{Pe_T} \frac{\partial C}{\partial x_1} = 0 \quad \text{at } x_1 = 0, \tag{8}$$

$$\frac{\partial C}{\partial x_1} = 0 \quad \text{at } x_1 = L, \tag{9}$$

$$\frac{\partial C}{\partial x_2} = -Pe_T U_s E_s \quad \text{at } x_2 = 0. \tag{10}$$

Modeling resuspension as a turbulent diffusive flux has the inconvenience of injecting energy into the current through particle diffusion: particles are lifted upward by diffusive effects without a corresponding energy loss. For small inclination angles and particle settling speed, ($\theta \leq 2°$, $U_s \leq 0.005$), this diffusive energy input may significantly affect the dynamics of the flow. For flat surfaces and small particle settling speeds, a more detailed description of the turbulence, such as that provided by a $K-\epsilon$ model (Speziale 1991), may help to account for this energy input by decreasing the turbulent kinetic energy and shall be investigated in the future. However, for larger slope angles, the potential energy lost or gained by the current through the deposition or resuspension of particles located higher than the downstream bottom boundary is much larger than that gained through particle diffusion. The dynamics of the flow are therefore dominated by the potential energy of deposited or resuspended particles and our model is expected to adequately describe currents evolving over sufficiently large slopes. Similarly, for large settling speeds, the energy lost through particle settling is dominant and our approach is expected to correctly capture the main features of the flow.

2.2. Numerical Approach

The numerical integration of equations (2)-(4) is performed in a manner similar to that of Härtel, Meiburg & Necker (2000). We perform a Fourier transform for ψ in the x_1-direction and use sixth order compact finite differences for other derivatives, except near the boundaries where the derivatives are accurate to third order (Lele 1992). A third order Runge-Kutta integrator is used to march equations (3)-(4) forward in time (Härtel *et al.* 2000). The velocity field is obtained by differentiating ψ. We use an adaptive time-step to satisfy the Courant-Friedrichs-Levy and diffusive stability criteria while minimizing computation time. We solve the governing equations over a rectangular domain described by $0 \leq x_1 \leq L$, $0 \leq x_2 \leq H$, with typical values $L = 24$ and $H = 4$ and a grid of size 1025×385. The flow is found to be unaffected by the choice of L as long as the tip of the current remains more than one non-dimensional unit away from the right wall. We investigate the influence of H in the following section.

Large concentration derivatives near the bottom boundary may result from the modeling of resuspension as a diffusive flux. A finer grid is thus required near the bed than in other areas of the computational domain. To accelerate computations, we have implemented an unevenly spaced grid in the x_2 direction. By considering a Taylor series expansion, we generalized the compact finite differences formulas presented in Lele (1992) to allow for the use of a varying Δx_2. An example of the resulting formula used to compute a first derivative is shown in the appendix. The obtained formulas are sixth order accurate and their local error scales as the sixth power of the local Δx_2. To determine the position of the grid points, x_2^j, we evenly space grid points on a stretching variable $0 \leq s^j \leq 1$ and use a mapping function of the form (Fletcher 1991)

$$x_2^j = H \frac{\tanh(\alpha(s^j - 1)) + \beta s^j + \tanh(\alpha)}{\tanh(\alpha) + \beta}$$

where typical values of the coefficients are $\alpha = 3$ and $\beta = 0.32$. These values yield $\Delta x_2 = 0.0028$ and $\Delta x_2 = 0.026$ near the bottom and top wall, respectively, with a continuous variation in the central region.

3. Simulation Results

We show in figure **??** typical concentration and vorticity fields associated with a particle-driven current computed via the model presented in §2. Here the current is traveling over a surface with a relatively large slope angle, $\theta = 5°$, and is therefore predominantly erosional. Resuspension increases the particle concentration near the bottom boundary (blue and black zones) to a level exceeding the initial concentration $C = 1$. Vortices are shed behind the head of the current and form nearly circular regions of non-zero particle concentration (yellow and green in figure **??**a) embedded in ambient fluid. Such vortices generate mixing with ambient fluid, causing the particle concentration to decrease below its initial value. They are also responsible for a significant fraction of the viscous energy dissipation and therefore act to reduce the kinetic energy of the current. The largest vorticity is found near the bottom boundary due to the no-slip boundary condition. The bottom shear stress is sufficiently large to cause particles to be reentrained. Behind the head of the current, vortices are seen to vertically mix the particle concentration. Fluid in the rear of the current tends to catch up with the front (Härtel *et al.* 2000), causing high particle concentrations to develop near the head.

3.1. Influence of the turbulent Reynolds and Péclet Numbers

We begin by studying the impact of the turbulent Reynolds number used in our simulations on the main features of the flow. Figure **??** shows the time evolution of the position of the front of a density current ($U_s = 0$) traveling over a horizontal surface. For relatively small turbulent Reynolds numbers, $Re_T < 1,000$, the front velocity increases significantly with Re_T. However this dependence becomes negligible for larger turbulent Reynolds numbers. For sufficiently large values of Re_T, other qualitative features of the flow, such as the shape and number of vortices shed behind the head or the size of the head, were also nearly independent of Re_T. The use of a reduced turbulent Reynolds number is thus expected to have only a small impact on the validity of our description of the fluid motion provided $Re_T > 1,000$.

The resuspension model, however, is more susceptible to the choice of $Re_T = Pe_T$. The non-dimensional bottom shear stress near a solid wall is known to decrease with increasing Reynolds number (Barenblatt 1993), which reduces resuspension for large values of Re_T. This may be understood by noting that increasing Re_T while keeping the non-dimensional settling speed constant corresponds to less vigorous turbulence, which is likely to generate less particle reentrainment. The magnitude of the turbulent Péclet number also influences the resuspended mass of particles. Our resuspension model spreads particles from the lower boundary over a thickness scaling as $\delta_r \sim Pe_T^{-1/2}$. Increasing Pe_T corresponds to reducing the strength of the turbulence and therefore causes the resuspended boundary layer to thin, leading to more deposition. The choice of Pe_T is analogous to that of the ratio of the bottom to the average particle concentration in layer averaged models (Parker *et al.* 1987). In particular, if $Re_T = Pe_T$ was varied by a factor of 2, a similar amount of resuspension was obtained when the particle radius changed by approximately 30%.

Although few measurements are available to allow us to determine an appropriate numerical value of $Re_T = Pe_T$ for realistic turbidity currents, it was found that setting $Re_T = Pe_T = 2,200$ qualitatively reproduces experimental data and agrees with previous models (García 1994). In particular, the size and density of particles subject to reentrainment ($\bar{d} \sim 100\mu$m, $\bar{\rho}_p \sim 2.5$g/cm^3) for a current of given velocity ($\sim$ 1m/s) are commensurate with available experimental data (García & Parker 1993, García 1994). Such a choice of turbulent Reynolds and Péclet number also allows us to maintain a manageable computation time.

It should also be noted that similar results were obtained when considering a simpler and cruder resuspension model. In our early simulations, the diffusive flux at the bottom boundary was set to zero and resuspended particles were simply added uniformly over a layer of uniform thickness, $\delta_r \approx 0.1$, near the bottom boundary. The added mass of resuspended particles was computed at every time step, $M_r(x_1) = E_s U_s \Delta t$, and the concentration was increased in the resuspension layer

$$C(x_1, x_2, t) = C'(x_1, x_2, t) + M_r/\delta_r, \qquad \text{if } 0 < x_2 < \delta_r$$

where C' was obtained by advancing in time equations (2-4). The general features of the flow agreed well with those observed when particles are resuspended through a diffusive flux. The dependence on Re_T was similar in both models and increasing δ_r was analogous to reducing Pe_T. The most important features of the flow, and in particular whether or not a flow is self-sustaining therefore appear to be independent of the details on the resuspension model.

3.2. Effect of the Computational Domain Height

We now investigate the influence of the computational domain height, H, on the propagation velocity of the current. Experiments show that light fluid back flow may significantly reduce the velocity of currents spreading in shallow surroundings (Huppert & Simpson 1980). Figure **??**a shows the progression of the nose of density currents ($U_s = 0$), defined as the furthest point in the x_1-direction where $C > 0.5$, traveling over a flat surface for different values of H. After a brief acceleration period, the velocity of the current's front remains nearly constant over the first 20 non-dimensional time units. At longer times, the current decelerates slowly as the height of its head decreases. Currents traveling in deep ambient fluid are not readily affected by the fluid back flow and thus travel faster downstream. Such currents also to shed significantly fewer vortices, and therefore to dissipate much less energy through viscous effects. It may be seen from figure **??**a that computations performed with $H \geq 4$ are not significantly influenced by the precise value of H and thus may be used to simulate gravity currents in very deep surroundings.

Figure **??**b shows the front velocity, u_f, of density currents propagating on slopes of constant angles in both shallow ($H = 2$) and deep ($H = 4$) computational domains.

In a deep ambient the front velocity is known experimentally to increase slightly with slope angle both for constant flux (Britter & Linden 1980) and constant initial volume (Beghin *et al.* 1981). Our simulations reveal a similar dependence of u_f on the slope angle. After an initial slumping phase, the currents travel at nearly constant speed, $u_f = 0.77$ for $\theta = 0°$, $u_f = 0.80$ for $\theta = 5°$ and $u_f = 0.83$ for $\theta = 10°$, showing a nearly linear dependence of the front velocity on θ. Significant mixing between the current and the ambient fluid is observed for large slope angles, reducing the velocity at later times as the size of the head decreases. In a shallow ambient, the slope angle has a negligible impact on the propagation velocity of the current (figure **??**b). Irrespectively of the slope angle, lighter fluid back flow hinders the progression of the current and generates numerous energy dissipating vortices.

3.3. Influence of the Initial Current Length

For resuspending currents, the time evolution of the mass of suspended particles is of primary importance in the description of the flow. If the mass of the currents increases in time, currents which we refer to as self-sustaining, the flow is mostly eroding and may travel for provided that the inclination angle remains sufficiently large. In contrast, currents traveling along relatively flat surfaces see their mass decrease in time and are mostly depositional. These currents quickly stop spreading as particles are deposited.

We proceed to investigate the influence of the initial current length, x_f, on the time evolution of gravity currents and in particular on their self-sustaining quality. Figure **??**a shows the time dependence of the mass of suspended particles of currents propagating over a small inclination angle, $\theta = 3°$, such that a current with $x_f = 2$

is depositional. Here the initial mass is normalized to one. The mass of suspended particles first increases briefly during the slumping phase of the current. However, at later times, the settling of particles exceeds resuspension and the total mass decreases. Increasing the initial length is seen to have no qualitative impact on the time dependence of the mass. The initial normalized mass increase is less for longer currents since the amount of resuspended particles near the front is nearly independent of x_f.

For a larger slope angle, $\theta = 4°$, a current with $x_f \geq 1$ becomes self-sustaining and its mass increases with time, see figure **??**b. Once again, the relative mass increase is smaller for longer currents. Notice that very short and tall currents, e.g. with $x_f = 0.5$ behave in a qualitatively different manner and appear mostly depositional. The initial length of the current therefore has little impact on its long term behavior, provided it is larger than a critical value near $x_f = 1$. In the remainder of the simulations presented here, we thus fix the initial current length equal to its initial height at $x_f = 2$.

3.4. Influence of Resuspension

Figure **??** shows an example of a strongly resuspending current. Here the slope angle is sufficiently large, $\theta = 5°$, and the particle settling speed sufficiently small, $U_s = 0.02$, so that the amount of resuspended particles exceeds that of deposited particles. Unresolved turbulent motions, modeled as a diffusive effect, are responsible for the high concentration observed below $x_2 \approx 0.1$, while the increase in particle concentration at higher levels is mostly attributable to the advection of the concentration through resolved fluid motions. As the current propagates downslope, its mass and velocity increase. In our system, the only saturation mechanism is the resuspension upper bound $E_s \leq 0.3/\bar{C}_0$, so the current may grow until the average particle concentration reaches a level where the average particle-particle interactions may not be neglected ($\bar{C} \sim 10\%$) and our model no longer applies.

In the early stages of motion (figure **??**a), the current resembles a non-eroding gravity current and only a small boundary layer at the bottom exhibits a larger particle concentration than $\bar{C}_0$. For comparison, we have included in figure **??**a an example of a current where the flow parameters are identical but resuspension is not taken into account ($E_s = 0$). In both cases, mixing with clear fluid dilutes the upper part of the current and the vortices shed behind the front are very similar. In the presence of resuspension, the particle concentration increases near the front and the formation of a massive head is observed (figures **??**c and e). The volume of the head does not change significantly as the current progresses, but it becomes denser, as illustrated by the integrated concentration profile, $< C >= \int_0^H C dz$, displayed in red in figure **??**b-d-f). The head becomes progressively heavier as resuspended particles accumulate near the front and it thus propagates faster, generating further erosion.

In the presence of resuspension, particles are deposited near the left wall, but strongly eroded near the initial front position, $x_f = 2$, as the initial slumping phase generates vigorous erosion (figure **??**b). Further downstream, $x_1 > x_f$, the erosion pattern is mostly flat in regions behind the current and increases nearly linearly toward the position of the nose of the current. The thin boundary layer preceding the bulk of the current indicates that the erosion process may begin ahead of the front of the current as motions in the ambient fluid are sufficiently vigorous to generate resuspension, The magnitude of the resuspension factor remains nearly constant, $E_s \approx 50$, and is close to saturation ($E_s < 0.3/\bar{C}_0 = 60$), in the regions where particle-laden fluid is present. The depth of the eroded region is thus approximately proportional to the time interval during which fluid overlies a given point and depends only weakly on the distance from the source. In the absence of resuspension, see figures **??**b-d-f, the deposit may only increase in time. The local height of the deposit reflects the time during which the current overlaid a given point.

3.5. Dependence of Mass and Velocity on Slope Angle

The slope angle, θ, plays a determinant role in the long term behavior of resuspending currents. For sufficiently large values of θ, the resuspended particles contribute significantly to the potential energy of the current and allow the current to become self-sustaining. Figure **??** shows the time evolution of the mass of suspended particles (a) and front velocity (b) of currents propagating at different slope angles. In the depositional regime ($\theta = 0°$, $\theta = 2°$), the mass of the current quickly decreases and shows little dependence on the slope angle. Similarly, the velocity of the front slowly decreases after a brief acceleration period. As particles settle out of suspension, the driving force is reduced and the front velocity decreases earlier than for a corresponding density current, see figure **??**.

For a larger slope angle ($\theta = 6°$), the mass increases in a nearly exponential fashion while it increases almost linearly for an intermediate angle ($\theta = 4°$). The slope angle is clearly seen to control the rate of increase, with larger slope angles generating significantly larger entrainment rates. Correspondingly, the front velocity increases with slope angle. As the head becomes denser, the pressure difference between the current and the ambient increases, thus giving rise to a larger driving force. For given flow parameters, there exists a critical slope angle, θ_c, above which the mass of the current increases in time and below which all particles eventually settle out. In the next section, we investigate the dependence of the critical angle of various flow parameters.

3.6. Self-Sustainment Criteria

We now wish to characterize the conditions under which a gravity current is self-sustaining. We consider only currents propagating in deep ambients, $H = 4$, and with initial aspect ratio equal to one ($x_f = 2$). We also fix the turbulent Péclet and Reynolds numbers, as well as the particle density and the fluid density and viscosity. We focus our attention on the effects of the initial (dimensional) height of heavy fluid, particle concentration and particle radius.

We first note that the particle flux at the lower boundary, $F = (-(\cos\theta)C|_{x_2=0} + E_s)U_s$, is allows to readily distinguish between the influence of the particle settling speed, U_s, and that of the resuspension factor, E_s. We find that if the resuspension factor is kept constant, the self-sustaining quality of the current is largely unaffected by changes in the particle settling speed. Changes in U_s influence the time scale over which particles settle or are resuspended but do not affect the mass balance directly. However, variations in the particle settling speed typically affect E_s and therefore, through the resuspension factor, influence the critical self-sustaining angle.

We present in figure **??** the dependence of the critical slope angle θ_c on the heavy fluid height and initial particle concentration in (a) and particle radius in (b). Here we keep $Re_T = Pe_T$ fixed, but we allow all other parameters to vary. The dimensional settling speed, buoyancy velocity, particle Reynolds number and resuspension factor are computed using the formulas of Dietrich (1982) and equations (1), (5) and (6), respectively, with varying values of $\bar{h}$, $\bar{d}$, and $\bar{C}_0$. As expected, large critical slope angle are associated with small values of $\bar{C}_0$ and $\bar{h}$ since these induce relatively low current velocities. As the current velocity increases through larger particle concentration or initial height, the non-dimensional settling speed diminishes, causing E_s to increase. The influence of $\bar{C}_0$ is weaker than that of $\bar{h}$; particle reentrainment will affect low particle concentration currents more readily as the relative particle concentration will then become larger, thus partially counteracting the fact that low values of $\bar{C}_0$ reduce the current velocity.

Figure ??b shows that increasing the particle radius renders resuspension more difficult since large particle radii cause E_s to decrease. For comparison, we show the dependence on particle size of a typical value of the inverse of the resuspension factor ($50/E_s$, scaled for plotting purposes). Both curves are nearly parallel, indicating that E_s is the determinant factor in the self-sustaining quality of a current. In the parameter regime investigated here, we therefore find, by fitting the curves shown in figures ??a-b, that currents are self-sustaining if

$$1 < K\frac{\sin\theta_c(\bar{h}\bar{C}_0)^{5/3}}{\bar{d}^{11/4}\bar{C}_0} \approx \frac{\sin\theta_c}{\sin 3.75^\circ}\frac{(\frac{\bar{h}}{1.6\text{m}}\frac{\bar{C}_0}{0.5\%})^{5/3}}{(\frac{\bar{C}_0}{0.5\%})(\frac{\bar{d}}{10^{-4}\text{m}})^{11/4}} \tag{11}$$

where K is a constant determined by the critical angle associated with our default parameter values $\bar{d} = 10^{-4}$m, $\bar{h} = 1.6$m and $\bar{C}_0 = 0.005$. Turbidity currents may thus be expected to grow in size as long as the inclination angle of the lower boundary is larger than θ_c, and to decay over regions where $\theta < \theta_c$.

3.7. Broken Slope Currents

We present here an application of our model to turbidity currents traveling down a slope of varying angle. To simulate the base of the continental slope, we selected a geometry where the initial slope is 5° and the surface away from the source is horizontal. The slope remains constant for $x_1 < 7$ and decreases linearly to 0° in the region $7 \leq x_1 < 9$. The current and particle parameters were chosen to cause the mass of the current to increase over the inclined region.

Figure **??** shows the progression of a current traveling down a broken slope. In the early stages of motion, the current is erosional and its concentration increases near the lower boundary. However, upon reaching the horizontal bed, the current becomes depositional and eventually comes to rest. The transition from flow over an incline to flow over a horizontal bottom surface occurs smoothly and no significant changes in the height of the current (hydraulic jump) is observed near the corner. The finite volume of heavy fluid presumably prevents us from observing steady hydraulic jumps such as those reported by García (1993).

Figure **??**a illustrates the dependence of the mass of suspended particles and front velocity on the position of the current tip. As the current travels downslope, its mass increases through erosion of the bed. The suspended mass continues to increase even after the nose has reached the flat surface, as most of the heavy fluid is still traveling downhill. At later times, all the heavy fluid overlies a horizontal surface and the current becomes depositional, causing the mass to decrease. The front velocity, after the initial slumping phase, increases while overlying a surface of sufficiently large slope angle. When the nose reaches the corner, the front velocity starts to decrease, showing that the local slope angle readily influences the front velocity. As the current spreads, the velocity keeps decreasing as particles are deposited.

The corresponding deposition pattern is presented in figure ??b for different times. Particles are deposited near the left wall before the eroding character of the current develops as it moves downstream. The depth of the eroded region remains constant over the region of large slope angle. Near the corner, the current enters a depositional regime and leaves a deposit of maximum height at the beginning of the flat region. The deposit then decreases with distance from the corner. If a current transports sufficient particles, the geometry of the bottom surface may therefore be significantly altered. In particular, the position of the corner is shifted to the left. The cumulative effect of successive turbidity currents could then displace or create large topographic features and have important geological consequences.

4. Conclusion

We have developed highly resolved simulations of resuspending currents traveling over a complex geometry. Our model allows for predictions of the erosion and deposition levels which are of interest in geological and industrial processes. The flexibility of our model allows us to consider how successive gravity currents may be influenced by the deposits left by earlier turbidity currents. We may therefore characterize the evolution of large scale deposit structures, which could eventually be used to locate oil and gas fields hosted by turbidites. In particular, we may simulate the spontaneous formation or damping of local bed topography and the evolution of the overall system topography.

The complexity of the problem at hand requires approximations in order to model realistic flows. The magnitude of the physical Reynolds number remains too large for direct numerical simulations to be performed and turbulent motions must therefore be approximated. However, we are now capable of simulating sufficiently high values of Re_T so that this shortcoming is expected to have only little impact on the description of the flow (Parsons & García 1998). We model the resuspension process empirically, due to the lack of an adequate theoretical model. The inclusion of resuspended particles as a turbulent diffusive flux renders the quantitative values presented here dependent on the choice of the turbulent Péclet number. However, the qualitative trends, in particular, the dependence of the critical self-sustaining angle on particle size or concentration, are independent of the value of Pe_T. Our model therefore captures the underlying physical processes correctly, but approximations of the resuspension process renders quantitative predictions difficult. Our results are consistent with comparable experimental results (García & Parker 1993, García 1994). In particular, resuspension becomes important for similar particle size ($\bar{d} \sim 100\mu$m) and non-dimensional settling speed ($U_s \sim 0.01$). Moreover, our study based on a simpler resuspension model where particles are added in a resuspension layer of fixed thickness shows that the qualitative features of the flow are independent of the details of the resuspension model.

For strongly resuspending currents, particle-particle interactions may become important. Currents propagating on a slope of large angle were seen to develop regions where the particle concentration exceeds 5%. The viscosity of the suspension (Huang & García 1998), as well as the particle settling speed would then be altered by the presence of neighboring particles (Richardson & Zaki 1954). Such effects were not included in our simulations as our main interest was to characterize the onset of self-sustainment, but they should be incorporated in simulations aiming to describe high particle concentration currents.

An important aspect to incorporate in future research is the polydispersity of the suspended particles, which may have a non-trivial influence on the self-sustaining character of a current. Our model may easily be extended to consider different particle sizes by keeping track of several particle concentrations. The concentration of particles in the bed must also be modeled since only the topmost particles, the so-called active layer, are available for resuspension (Parker *et al.* 2000). Armoring may then occur, where large deposited particles prevent the current from reentraining smaller underlying particles and prevents further growth of the current (Karim & Kennedy 1986). Studying the combined effects of polydispersity and repeated flows should lead to a better understanding of the formation of realistic deposits and will therefore be investigated in the near future.

Another potentially important aspect of the flow which was not taken into account in our study is the effect of variations in the span wise direction. Incorporating such effects requires three-dimensional simulations which remain very demanding computationally. However, from a theoretical point of view, our model may be expanded to simulate three-dimensional flows in a straightforward manner using the model described by Necker *et al.* (2003) for density currents. Given the appropriate computing resources, we could thus study the formation of three dimensional structures such as levees, canyons or mini-basins.

Acknowledgments. The authors gratefully acknowledge the financial support of BHP Billiton Petroleum.

References

Barenblatt, G.I., Scaling laws for fully-developed turbulent shear flows. 1. Basic hypotheses and analysis. *J. Fluid Mech., 248*, 513–520, 1993.

Beghin, P., E.J. Hopfinger, and R.E. Britter, Gravitational convection from instantaneous sources on inclined boundaries. *J. Fluid Mech., 107*, 407–422, 1981.

Blanchette, F., V. Piche, E. Meiburg, and M. Strauss, Evaluation of a simplified approach simulating gravity currents over slopes of varying angles. *Computers & Fluids*, submitted, 2004.

Bonnecaze, R.T., H.E. Huppert, and J.R. Lister, Particle–driven gravity currents. *J. Fluid Mech., 250*, 339–369, 1993.

Britter, R.E., and P.F. Linden, The motion of the front of a gravity current traveling down an incline. *J. Fluid Mech., 99*, 531–543, 1980.

Choi, S.U., and M.H. García, K-ϵ turbulence modeling of density currents developing two dimensionally on a slope. *J. Hydr. Eng., 128*, 55–63, 2002.

Dietrich, W.E., Settling velocity of natural particles. *Water Resources Res., 18(6)*, 1615–1626, 1982.

Fletcher, C.A.J., *Computational Techniques for Fluid Dynamics*, Volume 2. Springer, 2nd edition, 1991.

García, M.H., Hydraulic jumps in sediment–driven bottom currents. *J. Hydr. Engr., 119(10)*, 1094–1117, 1993.

García, M.H., Depositional turbidity currents laden with poorly sorted sediment. *J. Hydr. Engr., 120(11)*, 1240–1263, 1994.

García, M.H., and G. Parker, Entrainment of bed sediment into suspension. *J. Hydr. Eng., 117(4)*, 1991.

García, M.H., and G. Parker, Experiments on the entrainment of sediment into suspension by a dense bottom current. *J. Geophys. Res., 98*, 4793–4807, 1993.

Härtel, C., E. Meiburg, and F. Necker, Analysis and direct numerical simulation of the flow at a gravity current head. part 1. Flow topology and front speed for slip and no–slip boundaries. *J. Fluid Mech., 418*, 189–212, 2000.

Hay, A.E., R.W. Burling, and J.W. Murray, Remote acoustic detection of a turbidity current surge. *Science, 217*, 833–835, 1982.

Heezen, B.C., and M. Ewing, Turbidity currents and submarine slumps, and the 1929 Grand-Banks earthquake. *Am. J. Sci.*, 1952.

Hodson, M.E., The origin of igneous layering in the Nunarssuit Syenite, south Greenland. *Min. Magazine., 62(1)*, 9–27, 1998.

Hogg, A.J., M. Ungarish, and HE. Huppert, Particle-driven gravity currents: asymptotics and box-model solutions. *Eur. J. Mech. B-Fluids, 19*, 139–165, 2000.

Huang, X., and M.H. García, A Herschel-Bulkley model for mud flow down a slope. *J. Fluid Mech., 374*, 305–333, 1998.

Hughes-Clarke, J.E., A.N. Shor, D.J.W. Piper, and LA. Mayer, Large–scale current-induced erosion and deposition in the path of the 1929 Grand Banks turbidity current. *Sedimentology, 37*, 613–629, 1990.

Huppert, H.E., and J.E. Simpson, The slumping of gravity currents. *J. Fluid*

Mech., 99, 785–799, 1980.

Hutter, K., *Hydrology of disasters.* Chap 11. Kluwer Academic, 1996.

Karim, M.F., and J.F. Kennedy, Degradation of graded-material beds in sediment-deficient rivers. *Int. J. Sed. Res., 1*, 39–55, 1986.

Krause, D.C., W.C. White, D.J.W. Piper, and B.C. Heezen, Turbidity currents and cable breaks in the Western New Britain trench. *Geol. Soc. Am. Bull., 81*, 2153–2160, 1970.

Lele, S.K., Compact finite difference schemes with spectral–like resolution. *J. Comp. Phys., 103*, 16–42, 1992.

Necker, F., C. Härtel, L. Kleiser, and E. Meiburg, High–resolution simulations of particle–driven gravity currents. *Int. J. of Multiphase Flow, 28*, 279–300, 2002.

Necker, F., C. Härtel, L. Kleiser, and E. Meiburg, Mixing and dissipation in particle–driven gravity currents. submitted to *J. Fluid Mech.*, 2003.

Normark, W.R., H, Posamentier, and E. Mutti, Turbidite systems; state of the art and future directions. *Rev. of Geophys., 31*, 91–116, 1993.

Pantin, H.M., *Sand transport in rivers, estuaries and the sea*, chapter A model for ignitive autosuspension in brackish underflows, pages 283–290. Balkema, Rotterdam, 1991.

Pantin, H.M., In sediment transport and deposition by particulate gravity currents. In *IAS Special Publication 31*, 2001.

Parker, G., Y. Fukushima, and H. Pantin, Self–accelerating turbidity currents. *J. Fluid Mech., 171*, 145–181, 1986.

Parker, G., M.H. García, Y. Fukushima, and W. Yu, Experiments on turbidity currents over an erodible bed. *J. Hydr. Res., 25*, 191–244, 1987.

Parker, G., C. Paola, and S. Leclair, Probabilistic Exner sediment continuity equation for mixtures with no active layer. *J. Hydr. Eng., 126*, 818–826, 2000.

Parsons, J.D., and M.H. García, Similarity of gravity current fronts. *Phys. of Fluids, 10*, 3209–3213, 1998.

Pratson, L.F., and B.J. Coakley, A model for the headward erosion of submarine canyons induced by downslope-eroding sediment flows. *Geol. Soc. Am. Bull., 108*, 225–234, 1996.

Richardson, J.F., and W.N. Zaki, Sedimentation and fluidisation: Part I. *Trans. Inst. Chem. Eng., 32*, 35–53, 1954.

Shraiman, B.I., and E.D. Siggia, Scalar turbulence. *Nature, 405*, 639–646, 2000.

Simpson, J.E., *Gravity currents in the environment and the laboratory.* Cambridge University Press, 2nd edition, 1997.

Smith, J.D., and S.R. McLean, Spatially averaged flow over a wavy surface. *J. Geophys. Res., 82,*, 1735–1746, 1977.

Sparks, R.S.J., S.N. Carey, and H. Sigurdsson, Sedimentation from gravity currents generated by turbulent plumes. *Sedimentology, 38*, 839–856, 1991.

Speziale, C.G., Analytical methods for the developement of Reynolds-stress closures in turbulence. *Ann. Rev. of Fluid Mech., 23*, 107–157, 1991.

Spiegel, E.A., and G. Veronis, On the Boussinesq approximation for a compressible fluid. *Astrophys. J., 131*, 442–447, 1960.

Torquato, S., T. Truskett, and P.G. Debenedetti, Is random close packing of spheres well defined? *Phys. Rev. Lett., 84*, 2064–2067, 2000.

Zeng, J.J., D.R. Lowe, D.B. Prior, W.J. Wiseman, and B.D. Bornhold, Flow properties of turbidity currents in Bute inlet, British-Columbia. *Sedimentology, 38*, 965–996, 1991.

Appendix A: Finite-Difference Formula

We show here as an example, the formula obtained to estimate the first derivative of a function f for non-constant Δx_2

$$af'_{i-1} + f'_i + bf'_{i+1} = \alpha f_{i-2} + \beta f_{i-1} + \gamma f_i + \delta f_{i+1} + \epsilon f_{i+2}, \tag{A1}$$

where

$$\begin{aligned}
a &= \frac{x_{nn} x_p^2 x_{pp}}{(x_{nn} - x_n)(x_n + x_p)^2 (x_n + x_{pp})}, \\
b &= \frac{-x_n^2 x_{nn} x_{pp}}{(x_p - x_{pp})(x_{nn} + x_p)(x_n + x_p)^2}, \\
\alpha &= \frac{-x_n^2 x_p^2 x_{pp}}{(x_n - x_{nn})^2 x_{nn} (x_{nn} + x_p)^2 (x_{nn} + x_{pp})}, \\
\epsilon &= \frac{x_n^2 x_p^2 x_{nn}}{(x_p - x_{pp})^2 x_{pp} (x_n + x_{pp})^2 (x_{nn} + x_{pp})} \\
\beta &= x_{nn} x_p^2 x_{pp} \left(\frac{6x_n^3 - 2x_{nn} x_p x_{pp} + x_n^2(-5x_{nn} + 4x_p + 5x_{pp})}{x_n (x_n - x_{nn})^2 (x_n + x_p)^3 (x_n + x_{pp})^2} + \right. \\
&\quad \left. \frac{x_n(-3x_{nn} x_p - 4x_{nn} x_{pp} + 3x_p x_{pp})}{x_n (x_n - x_{nn})^2 (x_n + x_p)^3 (x_n + x_{pp})^2} \right) \\
\delta &= x_{nn} x_n^2 x_{pp} \left(\frac{-6x_p^3 + 2x_{nn} x_n x_{pp} + x_p^2(5x_{pp} - 4x_n - 5x_{nn})}{x_p (x_p - x_{pp})^2 (x_n + x_p)^3 (x_{nn} + x_p)^2} + \right. \\
&\quad \left. \frac{x_p(3x_{pp} x_n + 4x_{nn} x_{pp} - 3x_n x_{nn})}{x_p (x_p - x_{pp})^2 (x_n + x_p)^3 (x_{nn} + x_p)^2} \right) \\
\gamma &= \frac{2}{x_n} + \frac{1}{x_{nn}} - \frac{2}{x_p} - \frac{1}{x_{pp}}, \\
x_p &= x_2^{i+1} - x_2^i, \quad x_{pp} = x_2^{i+2} - x_2^i, \\
x_{nn} &= x_2^i - x_2^{i-2}, \quad x_n = x_2^i - x_2^{i-1}.
\end{aligned}$$

Similar formulas were obtained for second derivatives and approximations near and at the boundary.

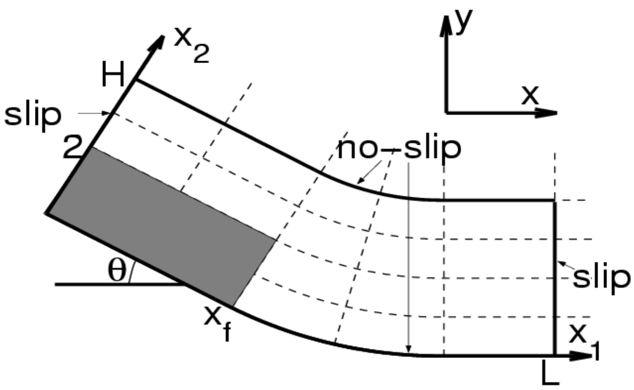

Figure 1. Schematic of the coordinate system used in our simulations. The angle θ between the x_1-axis and the horizontal is allowed to vary with x_1 to model varying slopes. The dark region corresponds to the initial position of the heavy fluid and is constrained by $0 \leq x_1 \leq x_f$, $0 \leq x_2 \leq 2$. The height and length of the computational domain are H and L, respectively.

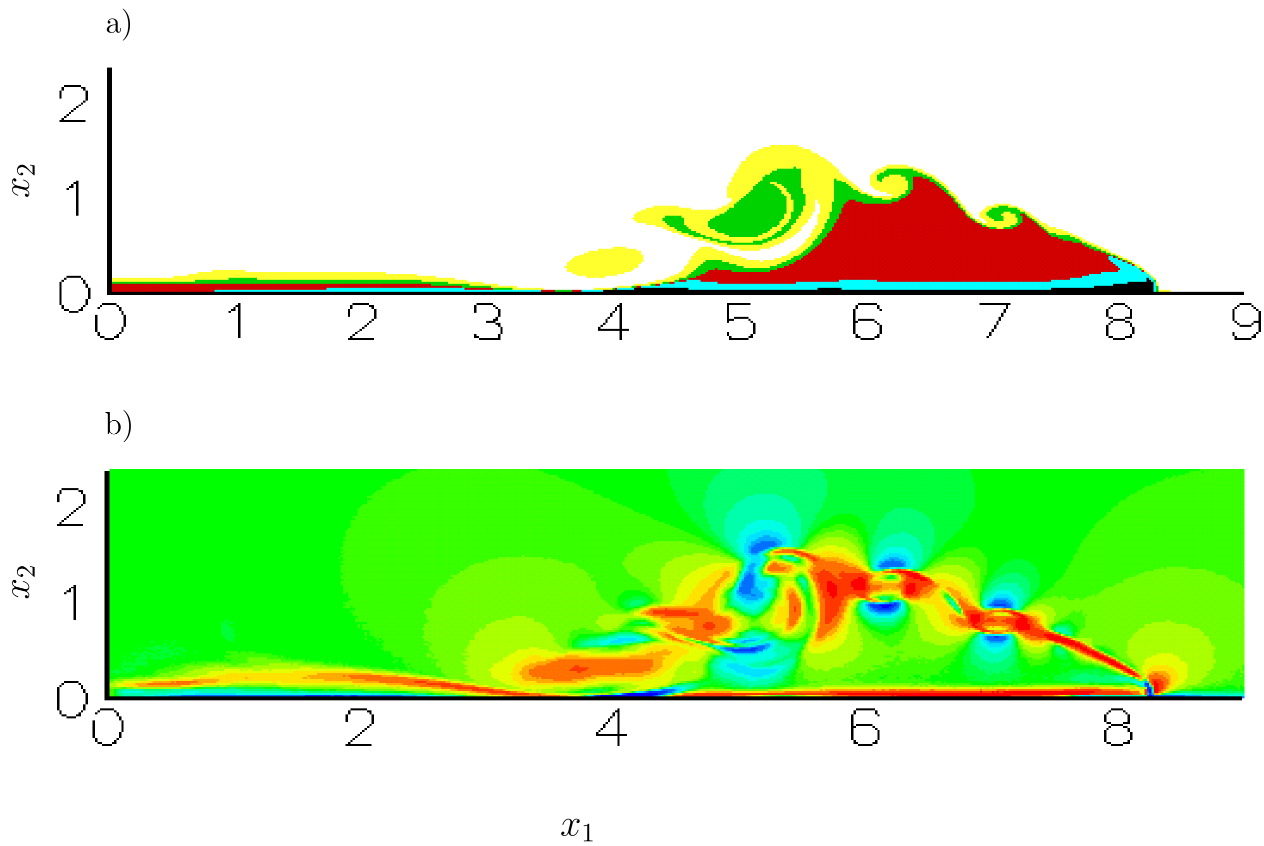

Figure 2. Sample of the concentration (a) and vorticity (b) of a particle-driven current traveling over a surface with an inclination angle $\theta = 5°$, at $t = 7.5$ computed via our numerical model. In (a), the color code is: $0.1 < C \leq 0.5$ yellow, $0.5 < C \leq 0.8$ green, $0.8 < C \leq 1$ red, $1 < C \leq 3$ cyan and $3 < C$ black. In (b), positive (counterclockwise), zero and negative (clockwise) vorticity are shown in red, green and blue respectively. The simulation parameters are $H = 4$, $L = 24$, $x_f = 2$, $U_s = 0.02$, $Re_p = 3.83$ and $Re_T = Pe_T = 2,200$.

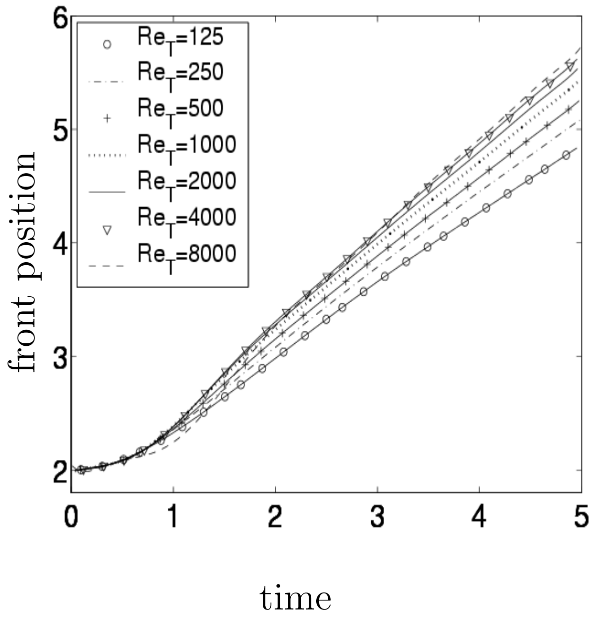

Figure 3. Time-dependence of the front position of a density current ($U_s = 0$) traveling over a horizontal surface for various values of the turbulent Reynolds number. For $Re_T \geq O(1,000)$, the front velocity becomes nearly independent of Re_T. Other parameters are $x_f = 2$, $H = 4$, $L = 12$ and $Pe_T = Re_T$.

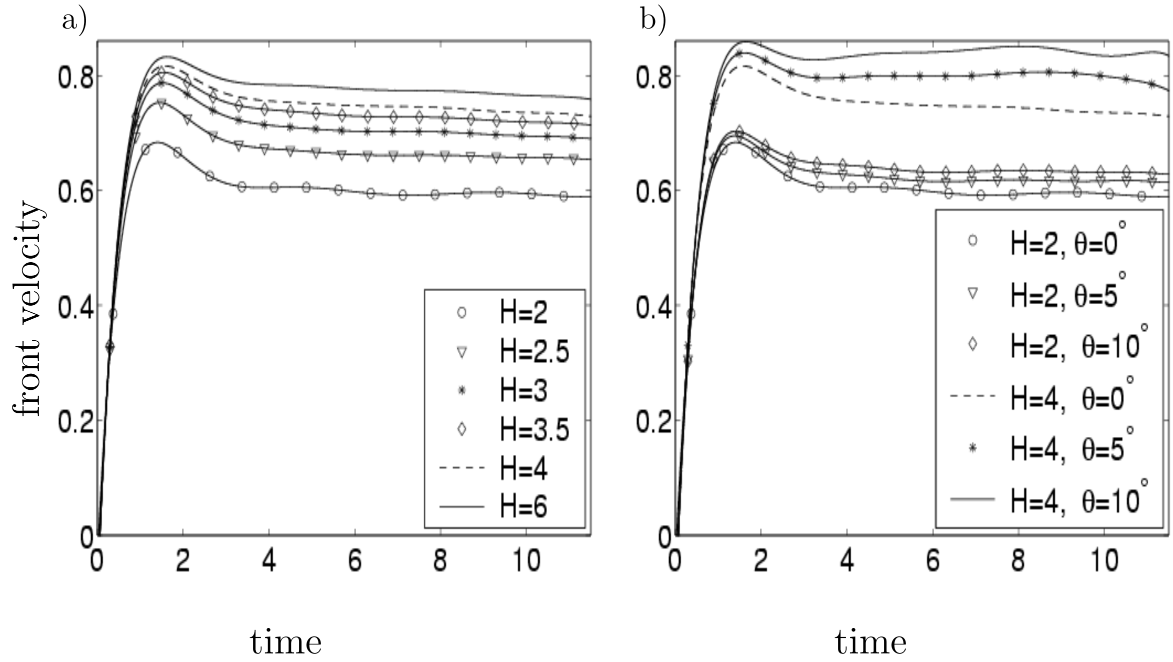

Figure 4. a) Time dependence of the front velocity, u_f, for different values of the computational domain height, H for a fixed initial heavy fluid height of 2. The dependence of the front velocity on H is relatively weak for $H \geq 4$. b) Time dependence of the front velocity for different inclination angles θ for both shallow, $H = 2$, and deep, $H = 4$, ambients. In these simulations, we consider density currents ($U_s = 0$) propagating over a horizontal surface with $Re_T = Pe_T = 2,200$ and initial length $x_f = 2$.

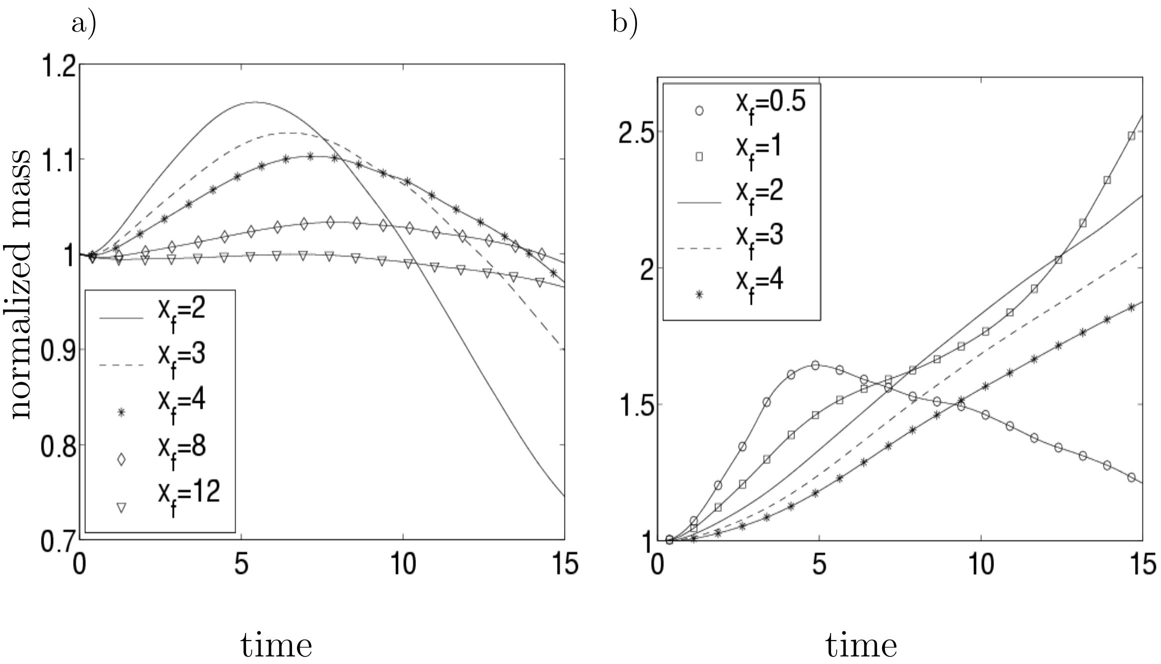

Figure 5. Time dependence of the current mass normalized by the initial mass for various initial length, x_f, at two different inclination angles, a) $\theta = 3°$ and b) $\theta = 4°$. Provided that $x_f \geq 1$, the long-term behavior of the current appears to be independent of the precise value of x_f. In these simulations, we consider deep-water particle-laden currents, $H = 4$, with $U_s = 0.02$, $Re_p = 3.83$ and $Re_T = Pe_T = 2,200$.

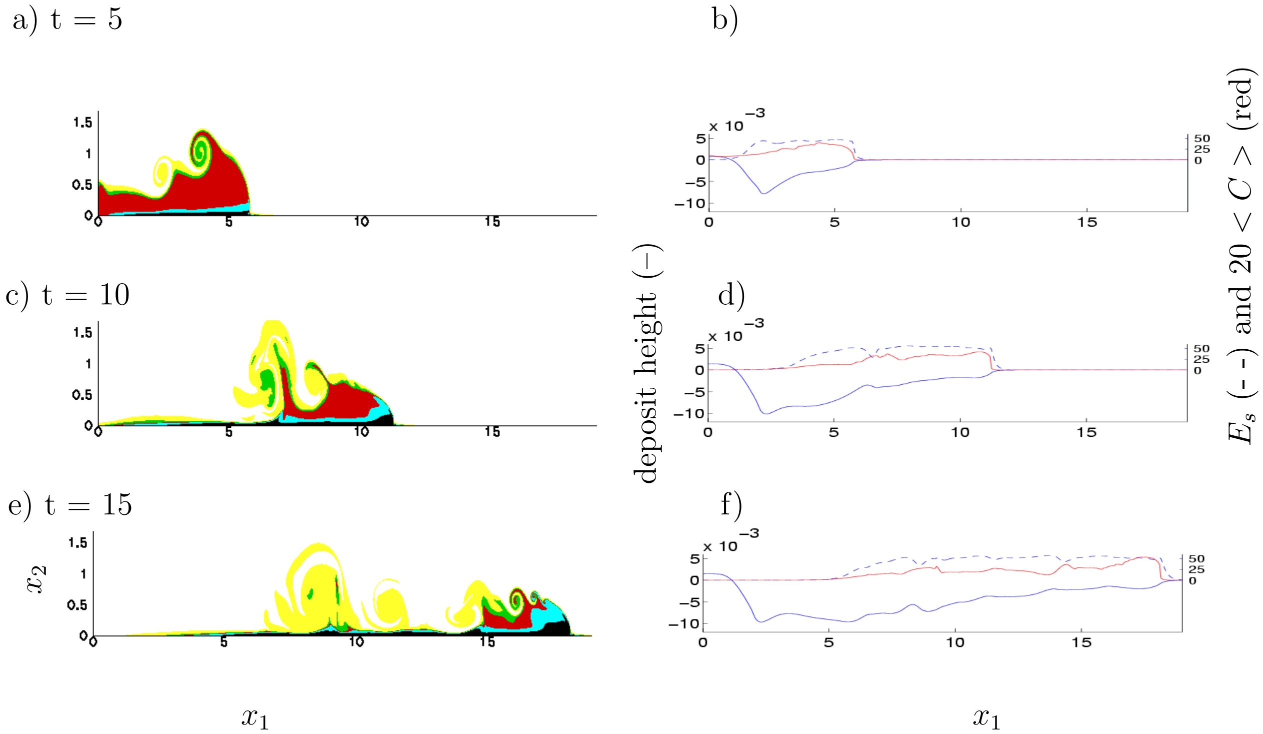

Figure 6. (a-c-e) Evolution of the particle concentration and (b-d-f) evolution of the bed height, resuspension factor E_s and average concentration $< C >= \int_0^H Cdz$, multiplied by 20 for scaling purposes, (red lines) of a strongly resuspending gravity current at times $t = 5$ (a-b), 10 (c-d) and 15 (e-f). The color code is: $0.1 < C \leq 0.5$ yellow, $0.5 < C \leq 0.8$ green, $0.8 < C \leq 1$ red, $1 < C \leq 3$ cyan and $3 < C$ black. In figures (b-d-f), the left scale refers to the bed height (solid lines) and the right scale to E_s (dashed lines) and $20 < C >$ (red lines). Other parameters are $\theta = 5°$, $\bar{d} = 100\mu$m, $\bar{h} = 1.6$m, $\bar{C}_0$=0.5%, $U_s = 0.02$, $Re_T = Pe_T = 2,200$, $x_f = 2$ and $H = 4$.

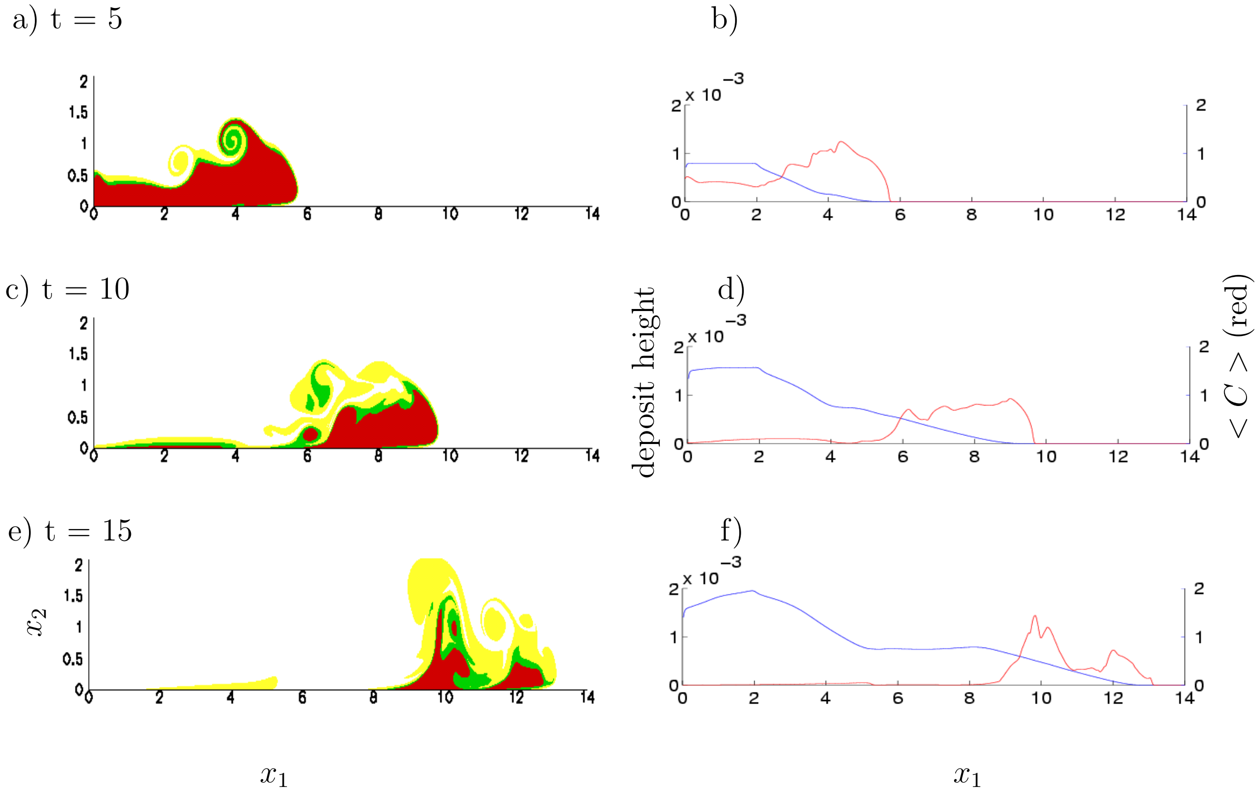

Figure 7. (a-c-e) Evolution of the particle concentration and (b-d-f) evolution of bed height (blue lines) and average concentration $< C >= \int_0^H C dz$, (red lines) of a non-resuspending gravity current at times $t = 5$ (a-b), 10 (c-d) and 15 (e-f). The color code is $0.1 < C \leq 0.5$ yellow, $0.5 < C \leq 0.8$ green, $0.8 < C \leq 1$ red. The flow parameters are as in figure **??**, $\theta = 5°$, $\bar{d} = 100\mu$m, $\bar{h} = 1.6$m, $\bar{C}_0$=0.5%, $U_s = 0.02$, $Re_T = Pe_T = 2,200$, $x_f = 2$, $H = 4$, but the resuspension factor E_s has been set to 0.

a) b)

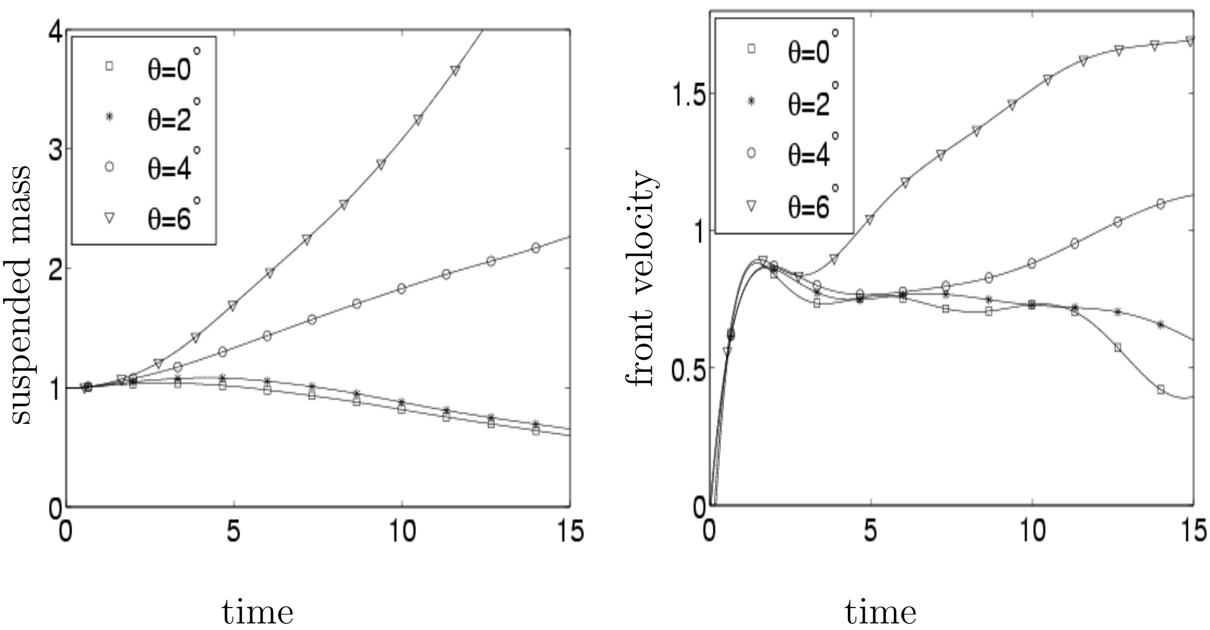

Figure 8. Time dependence of the (a) normalized mass of suspended particles and b) front velocity of currents propagating over slopes of various slope angle. A critical angle may be found, $\theta_c = 3.75°$, for which $\theta > \theta_c$ gives rise to currents whose mass increases indefinitely and $\theta < \theta_c$ generates depositional currents. Here the flow parameters are $Re_T = Pe_T = 2,200$, $x_f = 2$, $H = 4$, $\bar{d} = 100\mu$m, $\bar{h} = 1.6$m, $\bar{C}_0$=0.5% and $U_s = 0.02$.

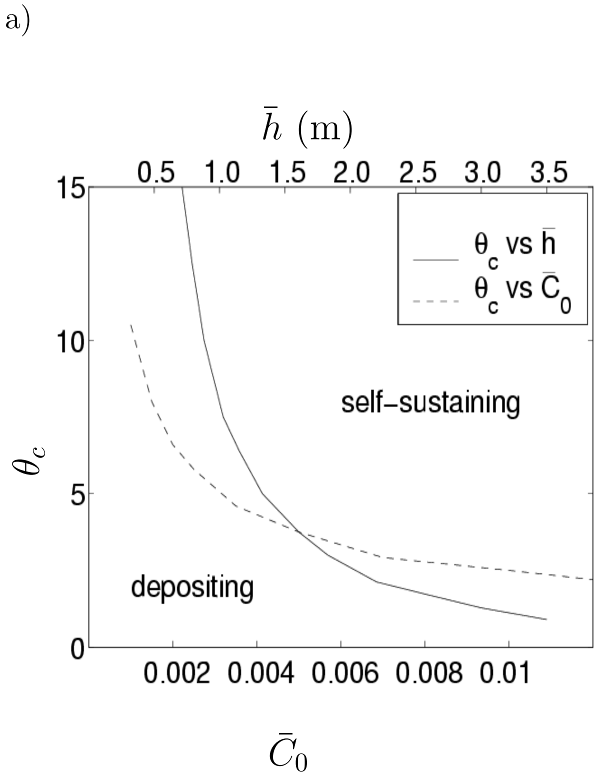

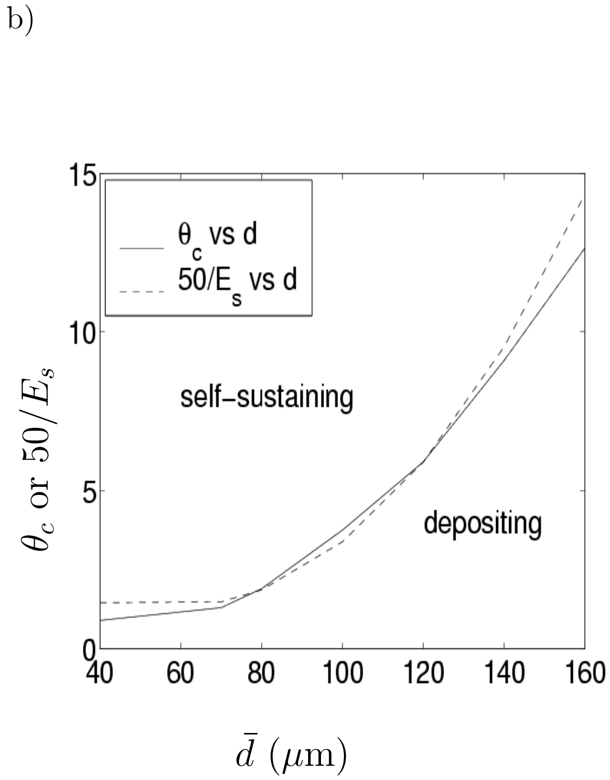

Figure 9. a) Dependence of the critical self-sustaining angle θ_c on the initial heavy fluid height, $\bar{h}$, (solid line, top scale) and on the initial particle concentration $\bar{C}_0$, (dashed line, bottom scale). b) Dependence of the critical angle on particle radius (solid line). For comparison, we show the dependence of $50/E_s$ on particle radius (dashed line), where E_s is the resuspension factor computed using a typical value of the shear velocity $u^* = 0.13$. Currents located above the curves are self-sustaining while those located below are depositional. The parameters used in these simulations are $Re_T = Pe_T = 2,200$, $x_f = 2$, $H = 4$, $\bar{d} = 100\mu$m, $\bar{C}_0 = 0.5\%$ and $\bar{h} = 1.6$m. The last three parameters are varied individually.

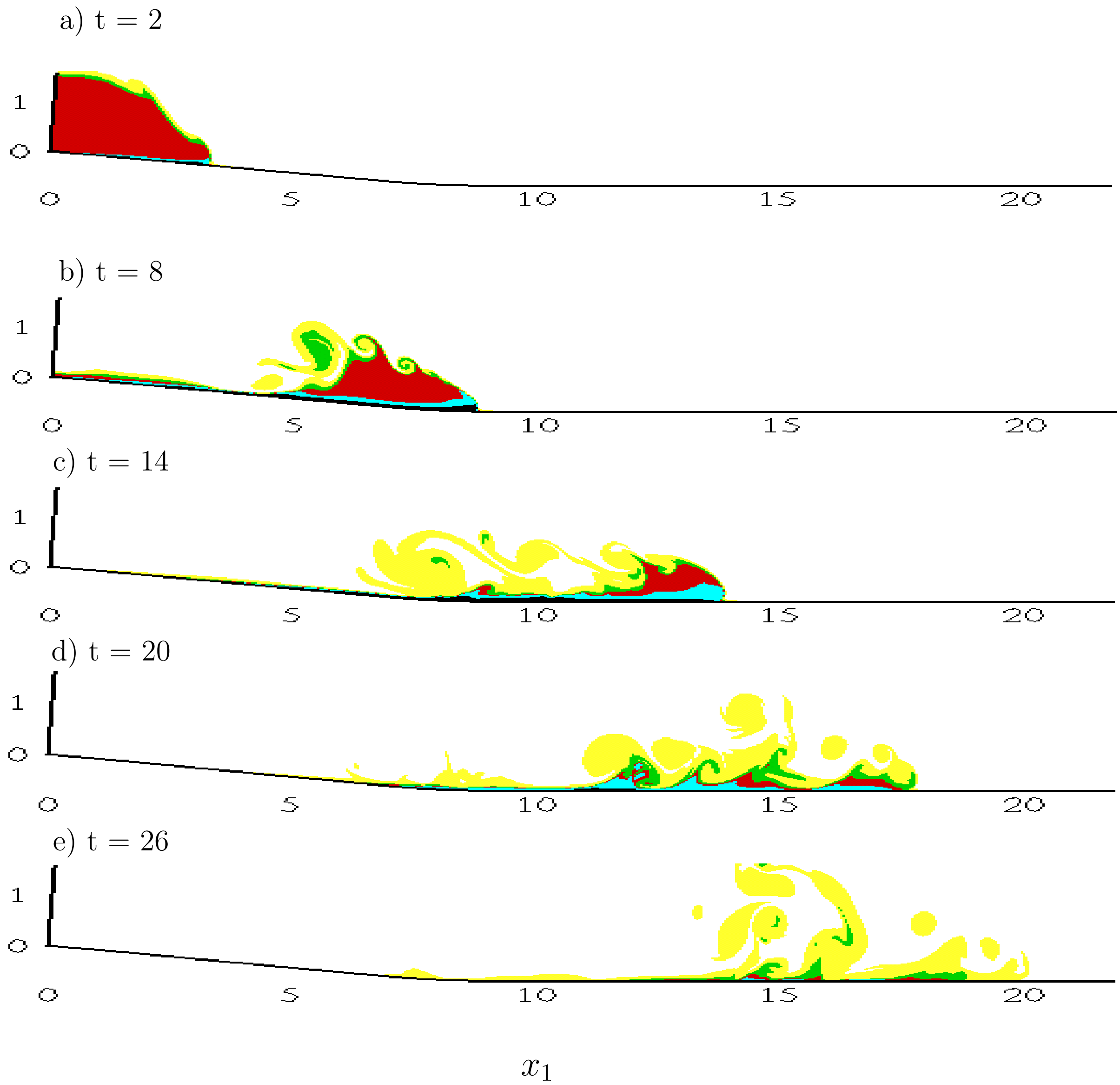

Figure 10. Particle concentration of a resuspending current traveling down a broken slope at times $t = 2$, 8, 14, 20 and 26. The initial slope angle is $\theta = 5°$ and the angle decreases linearly to 0 in the region $7 \leq x_1 < 9$. Corresponding current mass, velocity and particle deposits may be found in figure **??**. The color code is: $0.1 < C \leq 0.5$ yellow, $0.5 < C \leq 0.8$ green, $0.8 < C \leq 1$ red, $1 < C \leq 3$ cyan and $3 < C$ black. The flow parameters are again, $\bar{d} = 100\mu$m, $\bar{h} = 1.6$m, $\bar{C}_0$=0.5%, $U_s = 0.02$, $Re_T = Pe_T = 2,200$, $x_f = 2$, and $H = 4$.

a) b)

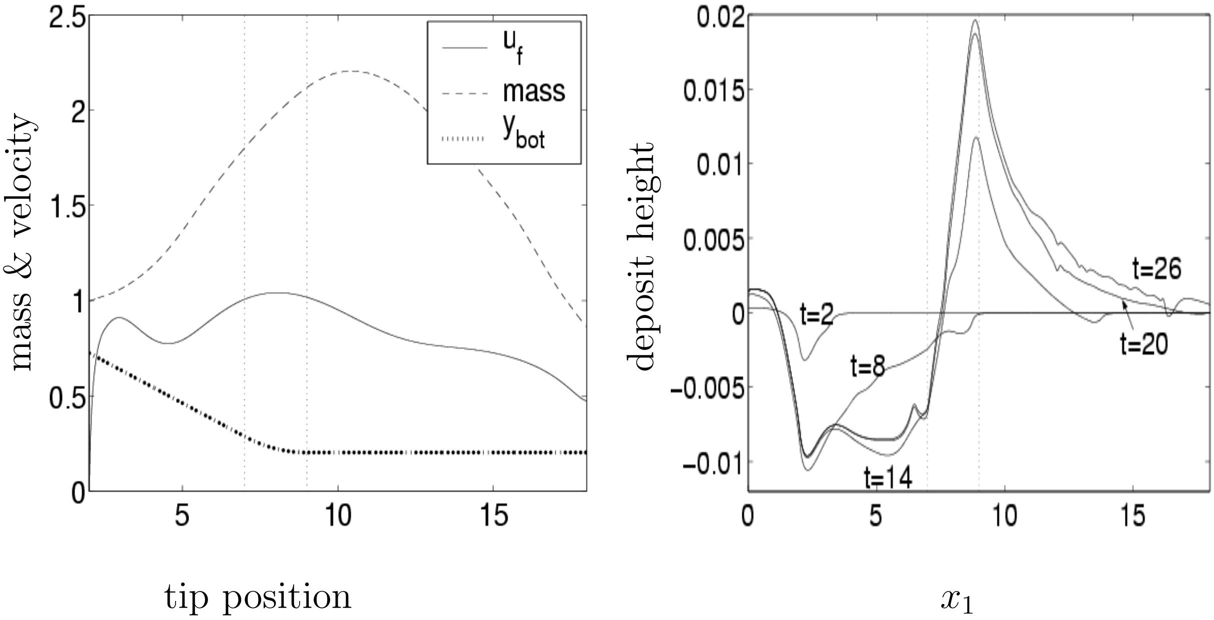

Figure 11. a) Front velocity (solid line) and suspended mass (dashed line) as a function of the position of the nose of a current propagating over a broken slope. The height of the bottom surface is shown as the dotted line. b) Dependence of the deposit height on the distance from the left wall at various times for the same current. The region left of the first vertical dotted line has a slope angle of $\theta = 5°$ and that right of the second line one of $\theta = 0°$. Other flow parameters are $Re_T = Pe_T = 2,200$, $x_f = 2$, $H = 4$, $\bar{d} = 100\mu$m, $\bar{h} = 1.6$m, $U_s = 0.02$ and $\bar{C}_0 = 0.5\%$.